ON MULTI-STATIC ADAPTIVE MICROWAVE IMAGING METHODS FOR EARLY BREAST CANCER DETECTION

Yao Xie, Bin Guo, Jian Li

University of Florida
Dept. of Electrical and Computer Engineering
P. O. Box 116130, Gainesville, FL 32611, USA.

Petre Stoica

Uppsala University
Dept. of Information Technology
Systems and Control Division
P.O. Box 337, SE-75105 Uppsala, Sweden.

ABSTRACT

We present two improved Multi-static Adaptive Microwave Imaging (MAMI) methods: MAMI-2 and MAMI-C, for early breast cancer detection. MAMI is one of the microwave imaging modalities based the significant contrast between the dielectric properties of normal and malignant breast tissues and employs multiple antennas that take turns to transmit ultra wideband (UWB) pulses while all antennas are used to receive the reflected signals. The MAMI methods we investigate herein utilize the data-adaptive robust Capon beamformer (RCB) to achieve high resolution and interference suppression. We will demonstrate the effectiveness of our proposed methods for breast cancer detection via numerical examples with data simulated using the finite difference time domain (FDTD) method based on a 3-D realistic breast model.

1. INTRODUCTION

Early diagnosis is currently the best hope of surviving breast cancer. Ultra-wideband (UWB) Confocal Microwave Imaging (CMI), based on the significant contrast in the dielectric properties between normal and malignant breast tissues [1], is one of the most promising and attractive new screening technologies. The idea of CMI is to transmit UWB pulses from antennas at different locations near the breast surface and reconstruct the image of the backscattered energy distribution coherently from the recorded backscattered responses.

The data acquisition approaches and the associated signal processing methods affect the CMI imaging quality. There are three major data acquisition schemes: mono-static, bi-static, and multi-static [2]. For multi-static CMI, each antenna in a real aperture array takes turns to transmit a probing pulse, and all antennas receive the backscattered signals. The multi-static approach can give better imaging results than its mono- or bi-static counterparts.

The challenge to CMI imaging is to devise signal processing algorithms to improve resolution and suppress strong interferences caused by the breast skin, nipple, etc. For multi-static ultra-wide band CMI, the data-independent DAS [3] and data-adaptive RCB based [2] signal processing algorithms have been considered. The data-adaptive methods can have better resolution and interference suppression capability than their data-independent counterparts.

In this paper, we propose two improved Multi-static Adaptive Microwave Imaging (MAMI) methods, i.e., MAMI-2 and MAMI-C, to form images of the backscattered energy for early breast cancer detection. For a focal point within the breast, the complete recorded multi-static data can be represented by a cube (Figure 1 (a)). In [2], we have proposed a MAMI approach, referred to MAMI-1 herein, which is a two-stage time-domain signal processing algorithm for multi-static CMI. In Stage I, MAMI-1 slices the data cube corresponding to each time index, and processes the data slice by the robust Capon beamformer (RCB) [4] to obtain backscattered waveform estimates at each time instant. Based on these estimates, in Stage II a scalar waveform is retrieved via RCB, the energy of which is used as an estimate of the backscattered energy for the focal point. MAMI-1 has been shown to have better performance than other existing methods [2]. MAMI-2 uses an alternative way of slicing the data cube in Stage I before applying RCB: selecting a slice corresponding to each transmitting antenna index. We will show that MAMI-2 tends to yield better images than MAMI-1 for high input Signal-to-Interference-Noise Ratio (SINR), but worse images at low SINR. Therefore we propose an combined method - MAMI-C, which yields good performance in all cases of SINR. We will demonstrate the performance of the MAMI methods using data simulated with the Finite Difference Time Domain (FDTD) method based on the 3-D hemispherical breast model.

2. DATA MODEL

We consider a multi-static imaging system, where K antennas are arranged on a hemisphere relatively close to the breast skin at known locations (see Figure 1 (b)). Before image formation, we preprocess the raw received signals to remove

This work was supported in part by the National Institutes of Health (NIH) Grant No. 1R41CA107903-1 and the Swedish Science Council (VR).

backscattered signals from skin by subtracting a calibration signal (formed by averaging all raw received signals), to align all the recorded signals from the focal point at location **r** (the focal point will be scanned in the entire breast volume to form a 3-D image) by time-shifting, and to compensate for the propagation loss of the signal amplitude (see [2] for details).

Let $y_{i,j}(t)$ denote the preprocessed backscattered signal generated by the probing pulse sent by the ith transmitting antenna and received by the jth receiving antenna, where t denotes the time sample. Our goal is to form a 3-D image of the backscattered energy $E(\mathbf{r})$ from the complete received data $\{y_{i,j}(t)\}$, on a grid of focal points **r** within the breast, with the scope of detecting the tumor. We model $y_{i,j}(t)$ as:

$$\begin{aligned} y_{i,j}(t) &= s_{i,j}(t) + e_{i,j}(t), \\ & i,j \in \{1,\cdots,K\}, \quad t \in \{0,\cdots,N-1\} \end{aligned} \tag{1}$$

where $s_{i,j}(t)$ represents the tumor response and $e_{i,j}(t)$ represents the residual term, which includes the thermal noise and the interference. To cast (1) in a form suitable for the application of RCB [4], we approximate the data model (1) by making different assumptions.

MAMI-1 approximates the data model (1) differently:

$$\mathbf{y}_i(t) = \mathbf{a}(t)s_i(t) + \mathbf{e}_i(t), \tag{2}$$

where $\mathbf{y}_i(t) = [y_{i,1}(t), \cdots, y_{i,K}(t)]^T$, $\mathbf{e}_i(t) = [e_{i,1}(t), \cdots, e_{i,K}(t)]^T$, and $s_i(t)$ denotes the backscattered signal (from the focal point at location **r**) corresponding to the probing signal from the ith transmitting antenna. The vector $\mathbf{a}(t)$ in (2) is the array steering vector, which is approximately equal to $\mathbf{1}_{K\times 1}$ since all the signals have been aligned temporally and their attenuations compensated for in the preprocessing step. In (2) we assume that the steering vector varies with t but be nearly constant with respect to i to simplify the problem slightly. It causes little performance degradations to our robust adaptive algorithms.

MAMI-2 approximates the data model (1) differently:

$$\mathbf{y}_i(t) = \mathbf{a}_i s_i(t) + \mathbf{e}_i(t), \tag{3}$$

where $\mathbf{a}_i$ denotes the steering vector, which is again approximately $\mathbf{1}_{K\times 1}$. In (3) we assume that the steering vector varies with i, but is constant with respect to t.

In practice, the steering vectors $\mathbf{a}(t)$ and $\mathbf{a}_i$ may be imprecise, in the sense that their elements may differ slightly from 1. The fact motivates us to consider using RCB for waveform estimation. We assume that the true steering vector $\mathbf{a}(t)$ or $\mathbf{a}_i$ lies in uncertainty spheres given by

$$\|\mathbf{a}(t) - \bar{\mathbf{a}}\|^2 \le \epsilon_1, \quad \text{and} \quad \|\mathbf{a}_i - \bar{\mathbf{a}}\|^2 \le \epsilon_2, \tag{4}$$

where ϵ_1 and ϵ_2 are the uncertainty size parameters, the choice of which should be made as small as possible. Also, the smaller the N or the larger the steering vector errors the larger the parameters should be. Such qualitative guidelines are usually sufficient since the performance of RCB does not depend very critically on the uncertainty size parameters [4].

3. MAMI-2

In Stage I, both MAMI-1 and MAMI-2 obtain K signal waveform estimates via RCB. In Stage I of MAMI-2, for the ith probing pulse, the true steering vector $\mathbf{a}_i$ can be estimated via the covariance fitting approach of RCB:

$$\begin{aligned} \max_{\sigma_i^2, \mathbf{a}_i} \sigma_i^2 \quad \text{subject to} \quad & \hat{\mathbf{R}}_{Y_i} - \sigma_i^2 \mathbf{a}_i \mathbf{a}_i^T \ge 0, \\ & \|\mathbf{a}_i - \bar{\mathbf{a}}\|^2 \le \epsilon_2, \end{aligned} \tag{5}$$

where σ_i^2 is the power of the signal of interest, and

$$\hat{\mathbf{R}}_{Y_i} = \frac{1}{N}\mathbf{Y}_i\mathbf{Y}_i^T \tag{6}$$

is the sample covariance matrix with

$$\mathbf{Y}_i = [\mathbf{y}_i(0), \mathbf{y}_i(1), \cdots, \mathbf{y}_i(N-1)], \quad \mathbf{Y}_i \in \mathcal{R}^{K\times N}. \tag{7}$$

By using the Lagrange multiplier method, the solution to this optimization problem is given by:

$$\hat{\mathbf{a}}_i = \bar{\mathbf{a}} - \left[\mathbf{I} + \nu\hat{\mathbf{R}}_{Y_i}\right]^{-1}\bar{\mathbf{a}}, \tag{8}$$

where $\nu \ge 0$ is the corresponding Lagrange multiplier that can be solved efficiently from the following equation (e.g., using the Newton method):

$$\left\|(\mathbf{I} + \nu\hat{\mathbf{R}}_{Y_i})^{-1}\bar{\mathbf{a}}\right\|^2 = \epsilon_2, \tag{9}$$

since the left side of (9) is monotonically decreasing in ν. Then we can apply the following weight vector to the received signals to obtain the corresponding signal waveform estimate of the backscattered signal (from the focal point **r**) for the ith probing signal (see [4] for details):

$$\hat{\mathbf{w}}_{2,i} = \frac{\|\hat{\mathbf{a}}_i\|}{K^{1/2}} \cdot \frac{\left[\hat{\mathbf{R}}_{Y_i} + \frac{1}{\nu}\mathbf{I}\right]^{-1}\bar{\mathbf{a}}}{\bar{\mathbf{a}}^T\left[\hat{\mathbf{R}}_{Y_i} + \frac{1}{\nu}\mathbf{I}\right]^{-1}\hat{\mathbf{R}}_{Y_i}\left[\hat{\mathbf{R}}_{Y_i} + \frac{1}{\nu}\mathbf{I}\right]^{-1}\bar{\mathbf{a}}}. \tag{10}$$

Note that (10) allows the sample covariance matrix to be rank-deficient. The beamformer output can be written as:

$$\hat{\mathbf{s}}_i = \left[\hat{\mathbf{w}}_{2,i}^T\mathbf{Y}_i\right]^T, \quad \hat{\mathbf{s}}_i \in \mathcal{R}^{N\times 1}, \tag{11}$$

Repeating the above process for $i = 1$ through $i = K$, we obtain K waveform estimates $\hat{\mathbf{S}}_2 = [\hat{\mathbf{s}}_1, \cdots, \hat{\mathbf{s}}_K]^T$,$\hat{\mathbf{S}}_2 \in \mathcal{R}^{K\times N}$.

Similarly, in Stage I of MAMI-1, we obtain a set of waveform estimates $\hat{\mathbf{S}}_1 = [\hat{\mathbf{s}}(0), \cdots, \hat{\mathbf{s}}(N-1)]$, $\hat{\mathbf{S}}_1 \in \mathcal{R}^{K\times N}$ (see [2] for details.)

Let $\{\hat{\mathbf{s}}_1(t)\}_{t=0,\cdots,N-1}$, and $\{\hat{\mathbf{s}}_2(t)\}_{t=0,\cdots,N-1}$ denote the columns of the matrices $\hat{\mathbf{S}}_1$ and $\hat{\mathbf{S}}_2$, respectively. Since all probing signals have the same waveform, we assume that the true backscattered signal waveforms are (nearly) identical. So in Stage II, we can employ RCB to recover a scalar waveform

$\hat{s}(t)$ from $\{\hat{\mathbf{s}}_1(t)\}$ or $\{\hat{\mathbf{s}}_2(t)\}$ (see [2] for more details on Stage II of MAMI-1; Stage II of MAMI-2 is similar). Finally, the backscattered energy $E(\mathbf{r})$ is computed as:

$$E(\mathbf{r}) = \sum_{t=0}^{N-1} \hat{s}^2(t). \tag{12}$$

4. MAMI-C

It is well-known that the errors in sample covariance matrices (for example, the $\hat{\mathbf{R}}_{Y_i}$ above) and the steering vectors cause performance degradations in adaptive beamforming [5]. Note that, on one hand, MAMI-2 uses more snapshots (viz. N) than MAMI-1 (viz. K) to estimate the sample covariance matrix. Hence the sample covariance matrix of MAMI-2 is more precise than that of MAMI-1. On the other hand, MAMI-1 employs RCB N times, whereas MAMI-2 uses RCB K times (recall that $N > K$), so there is more "room" for robustness in MAMI-1 than in MAMI-2, which means that MAMI-1 should be more robust to steering vector errors. Therefore, at high input SINR (when the sample covariance matrix errors are more important) we can expect MAMI-2 to perform better than MAMI-1, and vice versa at low input SINR (when the errors in the steering vector are critical).

The above discussions together with the numerical examples presented later on, motivates us to consider combining MAMI-1 and MAMI-2 to achieve good performance in all cases of SINR. In the combined method, which is referred to as MAMI-C, we use the two sets of K waveform estimates yielded by Stage I of MAMI-1 and Stage I of MAMI-2 simultaneously in Stage II (note that MAMI-1 and MAMI-2 have a similar Stage II). In this way the combined method increases the number of "fictitious" array elements from K to $2K$.

The combined set of estimated waveforms is denoted by $\hat{\mathbf{S}}_C = [\hat{\mathbf{S}}_1^T \quad \hat{\mathbf{S}}_2^T]^T$, $\hat{\mathbf{S}}_C \in \mathcal{R}^{2K\times N}$. Stage II of MAMI-C consists of recovering a scalar waveform from the columns of $\hat{\mathbf{S}}_C$, which we denote as $\{\hat{\mathbf{s}}(t)\}_{t=0,\cdots,N-1}$. The vector $\hat{\mathbf{s}}(t)$ is treated as a snapshot from a $2K$-element (fictitious) "array":

$$\hat{\mathbf{s}}(t) = \mathbf{a}_C s(t) + \mathbf{e}_C(t), \quad t = 0, \cdots N-1, \tag{13}$$

where $\mathbf{a}_C$ is assumed to belong to an uncertainty set centered at $\tilde{\mathbf{a}} = \mathbf{1}_{2K\times 1}$, and $\mathbf{e}_C(t)$ represents the estimation error. Using RCB, we estimate $\mathbf{a}_C$ and then obtain the adaptive weight vector via an expression similar to (10):

$$\hat{\mathbf{w}}_C = \frac{\|\hat{\mathbf{a}}_C\|}{K^{1/2}} \cdot \frac{(\hat{\mathbf{R}}_C + \frac{1}{\mu}\mathbf{I})^{-1}\tilde{\mathbf{a}}}{\tilde{\mathbf{a}}^T(\hat{\mathbf{R}}_C + \frac{1}{\mu}\mathbf{I})^{-1}\hat{\mathbf{R}}_C(\hat{\mathbf{R}}_C + \frac{1}{\mu}\mathbf{I})^{-1}\tilde{\mathbf{a}}}, \tag{14}$$

where μ is the corresponding Lagrange multiplier, and $\hat{\mathbf{R}}_C$ is the following sample covariance matrix of $\hat{\mathbf{S}}_C$ defined similar to (6). The beamformer output gives an estimate of the signal of interest:

$$\hat{s}(t) = \hat{\mathbf{w}}_C^T \hat{\mathbf{s}}(t). \tag{15}$$

Finally, the backscattered energy at location $\mathbf{r}$ is computed using (12).

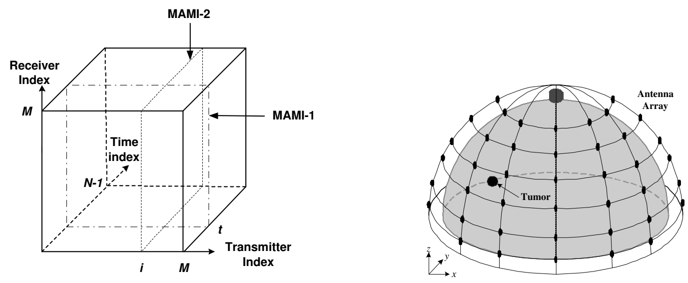

(a) (b)

Fig. 1. (a): multi-static CMI data cube model; (b): antenna array configuration.

5. NUMERICAL EXAMPLES

We consider a 3-D breast model as in [2] in our numerical examples. The 10 cm-diameter hemispherical breast model, including randomly distributed fatty breast tissue, glandular tissue, 2 mm thick breast skin, nipple, and chest wall, are designed to represent the physical non-homogeneity of the human breast. A 6mm (or 4 mm) in diameter tumor is located 2.7 cm under the skin (at $x = 70$ mm, $y = 90$mm, $z = 60$ mm). We assume that the dielectric properties (permittivity and conductivity) of the breast tissues are random distributed around their reported typical values (see also Table 2 of [2].) The dispersive properties of the breast tissues are modelled according to a single-pole Debye model.

As shown in Figure 1, the antenna array consists of $K = 72$ elements that are arranged on a hemisphere 1 cm away from the breast skin, on 6 layers with 12 antennas on each layer. Each antenna of the array takes turns to transmit a Gaussian probing pulse (an UWB pulse with frequency range from near DC up to 5 GHz), and all 72 antennas are used to receive the backscattered signals, which is simulated using FDTD method. The grid cell size used is 1 mm $\times$ 1 mm $\times$ 1 mm and the time step is 1.667 ps. Each preprocessed signal has $N = 150$ snapshots.

The performance comparisons of MAMI-1 with other existing methods can be found in [2]. Our examples focus on comparing MAMI-1 with the other two MAMI methods. In the following examples, we add white Gaussian noise with zero-mean and different variance values σ_0^2 to the received signals. We define SINR as:

$$10\log_{10}\left\{\frac{\frac{1}{K^2}\sum_{i=1}^{K}\sum_{j=1}^{K}\left[\frac{1}{N}\sum_{t=0}^{N-1}\breve{x}_{i,j}^2(t)\right]}{\frac{1}{K^2}\sum_{i=1}^{K}\sum_{j=1}^{K}\left[\frac{1}{N}\sum_{t=0}^{N-1}\breve{I}_{i,j}^2(t)\right]+\sigma_0^2}\right\}\text{dB},$$

where $\breve{x}_{i,j}(t)$ is the received signal due to the tumor only, and $\breve{I}_{i,j}(t)$ is due to the interference (without tumor response). We

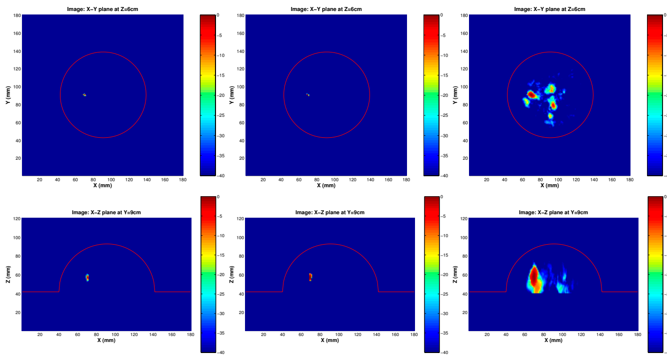

(a) MAMI-C (b) MAMI-2 (c) MAMI-1

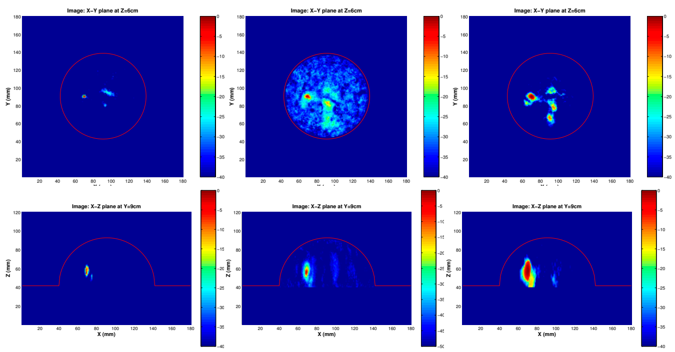

(d) MAMI-C (e) MAMI-2 (f) MAMI-1

Fig. 2. The images of the 4 mm - diameter tumor, (a), (b), and (c): at SINR = -12.5 dB; (e), (f), and (g): at SINR = -24.8 dB.

performed the simulation twice, with and without the tumor, regarded the second set of received signals as $\check{I}_{i,j}(t)$, and used their difference as $\check{x}_{i,j}(t)$. All the images are displayed on a logarithmic scale with a dynamic range of 40 dB.

Our numerical examples show that MAMI-C can detect 6mm-diameter tumor successfully in all cases of SINR. Due to space limit, herein we will only show the reconstructed images of 4mm-diameter tumor with different thermal noise levels. The backscattered microwave energy, which is proportional to the square of the tumor diameter, is much less in this case than in the 6mm-diameter tumor case, which presents a challenge to any image formation algorithm. In Figure 2 (a), Figure 2 (b), and Figure 2 (c), at a low noise level (SINR = -12.5 dB), MAMI-2 and MAMI-C yield images of comparable qualities and they outperform MAMI-1. Figure 2 (d), Figure 2 (e), Figure 2 (f), shows the images produced via the MAMI methods at a high noise level (SINR = -24.8 dB). Once again, MAMI-C yields the best images.

Figure 3 presents the 3-D images of the 4 mm-diameter tumor, for the low noise level cases. The 3-D images illustrate the reconstructed backscattered energy outside the two cross-sectional planes. The conclusions drawn from Figure 3 are similar to those from Figure 2.

6. CONCLUSIONS

We have presented two improved multi-static adaptive microwave imaging (MAMI) methods - MAMI-2 and MAMI-C - for early breast cancer detection. The MAMI methods utilize the data-adaptive robust Capon beamformer (RCB) to achieve high resolution and interference suppression. We have demonstrated the effectiveness of the MAMI methods for early breast cancer detection via numerical examples with data simulated using the finite difference time domain method based on a 3-D realistic breast model. We have shown that the MAMI-C method can detect tumors as small as 4 mm in diameter based on the realistically simulated 3-D breast model.

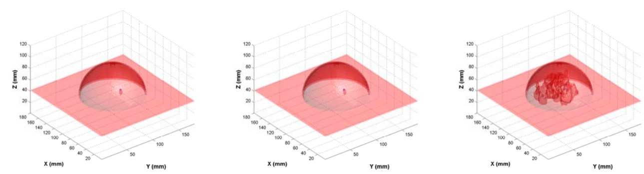

(a) MAMI-C (b) MAMI-2 (c) MAMI-1

Fig. 3. The 3-D images of the 4 mm - diameter tumor, at SINR = -12.5 dB.

7. REFERENCES

[1] C. Gabriel, R. W. Lau, and S. Gabriel, "The dielectric properties of biological tissues: II. measured in the frequency range 10Hz to 20GHz," *Physics in Medicine and Biology*, vol. 41, no. 11, pp. 2251–2269, November 1996.

[2] Y. Xie, B. Guo, L. Xu, J. Li, and P. Stoica, "Multi-static adaptive microwave imaging for early breast cancer detection," *39th ASILOMAR Conference on Signals, Systems and Computers*, Pacific Grove, CA, October 2005.

[3] R. Nilavalan, A. Gbedemah, I. J. Craddock, X. Li, and S. C. Hagness, "Numerical investigation of breast tumour detection using multi-static radar," *IEE Electronics Letters*, vol. 39, no. 25, December 2003.

[4] J. Li, P. Stoica, and Z. Wang, "On robust Capon beamforming and diagonal loading," *IEEE Transactions on Signal Processing*, vol. 51, no. 7, pp. 1702–1715, July 2003.

[5] D. D. Feldman and L. J. Griffiths, "A projection approach for robust adaptive beamforming," *IEEE Transactions on Signal Processing*, vol. 42, pp. 867–876, April 1994.